Neuron 50, 145–157, April 6, 2006 ©2006 Elsevier Inc. DOI 10.1016/j.neuron.2006.02.023

Temporal Encoding of Place Sequences by Hippocampal Cell Assemblies

George Dragoi[1,2,*] and György Buzsáki[1,*]
[1] Center for Molecular and Behavioral Neuroscience
Rutgers, The State University of New Jersey
Newark, New Jersey 07102
[2] Picower Institute for Learning and Memory
Massachusetts Institute of Technology
Cambridge, Massachusetts 02139

Summary

Both episodic memory and spatial navigation require temporal encoding of the relationships between events or locations. In a linear maze, ordered spatial distances between sequential locations were represented by the temporal relations of hippocampal place cell pairs within cycles of theta oscillation in a compressed manner. Such correlations could arise due to spike "phase precession" of independent neurons driven by common theta pacemaker or as a result of temporal coordination among specific hippocampal cell assemblies. We found that temporal correlation between place cell pairs was stronger than predicted by a pacemaker drive of independent neurons, indicating a critical role for synaptic interactions and precise timing within and across cell assemblies in place sequence representation. CA1 and CA3 ensembles, identifying spatial locations, were active preferentially on opposite phases of theta cycles. These observations suggest that interleaving CA3 neuronal sequences bind CA1 assemblies representing overlapping past, present, and future locations into single episodes.

Introduction

A challenging goal in neuroscience is to understand how a particular neuronal mechanism that evolved for a given function at an earlier stage of evolution can be employed for another function in subsequently evolved brains. In humans, the hippocampus and associated structures are believed to support episodic and semantic memories (Scoville and Milner, 1957; Tulving, 1972; Squire, 1992; Eichenbaum et al., 1999). In contrast, work on rodents suggests that these same structures play a critical role in map-based spatial navigation (O'Keefe and Nadel, 1978; Hafting et al., 2005) and/or dead reckoning navigation/"path integration" (McNaughton et al., 1996; Redish and Touretzky, 1997). Neuronal mechanisms of path integration and episodic memory are related because both processes require a coordinated integration of sequential information in a spatial-temporal context.

Sequential activation of hippocampal place cells on a track is believed to require a temporal context, as indicated by the systematic relationship between spike timing and the phase of the ongoing theta oscillation in the rat (O'Keefe and Recce, 1993). As the rat enters the receptive field of the neuron, the spikes occur on the peak of the theta cycle recorded at the CA1 pyramidal layer and may precess a full period as the rat passes through the entire receptive field of the cell. One explanation of the "phase precession" phenomenon is the interaction between two inputs to place cells ("pacemaker" model). One input represents environmental information, whereas the exact timing is paced by a rhythmic theta oscillation to all neurons, presumably from the septal pacemaker (O'Keefe and Recce, 1993; Skaggs et al., 1996; Mehta et al., 2002; Harris et al., 2002). A consequence of the pacemaker model is a predictable temporal relationship between different place cells within the theta cycle, even if place cells do not interact with each other (Skaggs et al., 1996). An implication of this hypothesis is that the best prediction of the rat's position is reflected by the phase-place correlation of the recorded multiple "independent" cells (Huxter et al., 2003). Because the pacemaker model does not require synaptic interactions among place cells, the variability of the space-spike phase relationship across subsequent trials is considered to be "noise." Therefore, the "ideal" phase for each trial would be the average phase value of all trials. Alternatively, sequential segments of the track are represented by unique sets of cell assemblies, which are bound together by synaptic interactions into an episode (Tsodyks et al., 1996; Jensen and Lisman, 1996). This organization implies temporally coordinated activity within and between anatomically distributed groups of sequential cell assemblies (Hebb's "phase sequence") (Hebb, 1949). According to the latter (assembly) model, phase precession of spikes within the theta cycle would result from the intrinsic oscillatory dynamics of the hippocampal formation in the framework of an attractor dynamical systems model (Tsodyks et al., 1996; Jensen and Lisman, 1996; Wallenstein and Hasselmo, 1997; Samsonovich and McNaughton, 1997; Wills et al., 2005). In the assembly model, spike phase variability of the place cells are temporally correlated because timing of neuronal action potentials depends on the activity of the synaptically connected cell assemblies in which individual cells are embedded. To address these competing hypotheses, we recorded from hippocampal CA1 and CA3 neuronal ensembles as the animals explored a rectangular elevated track for food reward (Dragoi et al., 2003), and we examined the temporal correlations between cell pairs in various aspects of the task. The findings support an internally coordinated assembly model and show that the most active assembly, representing the current location/item and anchored to the trough of the local theta cycle, is bound with the surrounding assemblies, representing past and future locations/items.

Results

Representation of Spatial Distances by Temporal Correlation

We recorded from hippocampal CA1 and CA3 neurons (n = 256 in four rats) during navigation on a rectangular elevated track for food reward (Dragoi et al., 2003).

*Correspondence: gdragoi@mit.edu (G.D.); buzsaki@axon.rutgers.edu (G.B.)

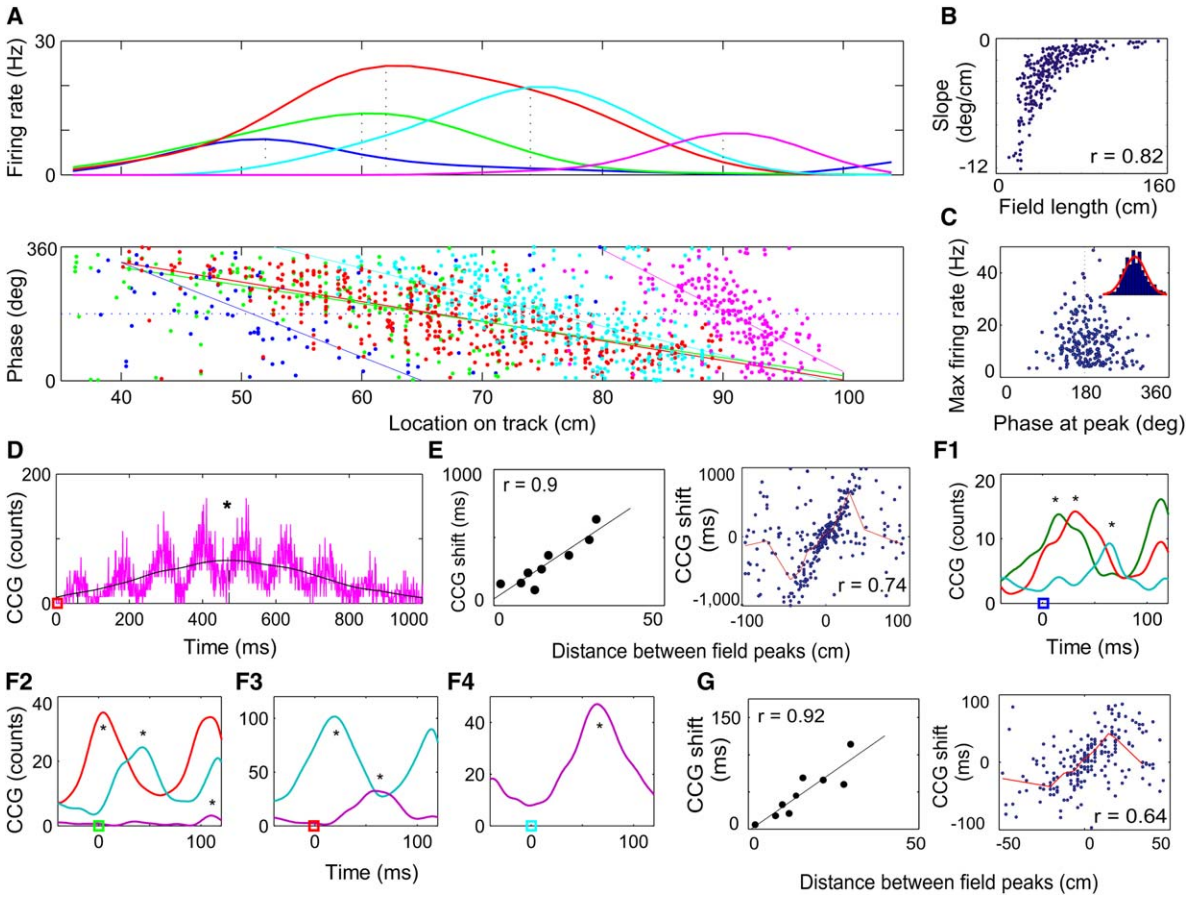

Figure 1. Representation of Place Sequences by Temporal Correlation

(A) Encoding of spatial location in five sequential place cells (color coded) by rate (top) and phase precession (bottom). Lines, position-phase regression slopes.

(B) Significant position-phase linear regression slopes as a function of place field length (n = 270 fields).

(C) Relationship between median phase at field peak and firing rate. Inset: normal distribution of median phase at place field peak (mean is at 180°).

(D) Cross-correlogram (CCG) between two cells (orange cell at time zero versus magenta cell). Note theta frequency modulation over nine cycles in 1 s. Star, peak of the smoothed (line) cross-correlogram at 470 ms.

(E) Time differences, determined by the peaks of the smoothed CCG of the nine cell pair combinations (left) and all pairs (right), as a function of distance between field peaks, determined by the peak firing rates of the individual neurons ("coding by real-time scale"). Red line, running median.

(F) Cross-correlograms (CCG) between blue (reference) cell versus green, orange, and cyan (partner) neurons at a short (theta) scale (F1) and between other pairs ([F2–F4], color squares, reference neuron). Stars, peaks of cross-correlograms.

(G) Time differences, determined by the peaks of the short time scale CCG of the nine cell-pair combinations (left) and all pairs (right), as a function of distance between field peaks ("coding by theta time scale").

Figure 1 illustrates a typical sequential activation of place cells with partially overlapping place fields (Jensen and Lisman, 1996). As shown earlier, the spatial position of the animal correlated with both the firing rates (O'Keefe and Nadel, 1978) of hippocampal pyramidal neurons (Figure 1A, top) as well as the phase of spikes within the theta cycle (O'Keefe and Recce, 1993; Huxter et al., 2003) (Figure 1A, bottom). Thus, the spike phase information provided an estimate of the distance traveled from the beginning of the place field for a given neuron. This distance information was cell specific rather than expressed in an absolute metric, since the slope of the spike phase shift depended on the size of the place field (Figure 1B; see also Huxter et al., 2003). Therefore, the distances between sequentially visited places cannot be accurately calculated solely from the phase precession of individual place cells.

The current position of the animal is defined by the maximum firing activity of a population of place cells (Wilson and McNaughton, 1993). Peak firing rates of hippocampal pyramidal neurons were anchored to the trough of the locally recorded theta cycle (Figures 1A and 1C), as if the trough functioned as an attractor for the assembly representing the current position (Wallenstein and Hasselmo, 1997; Tsodyks, 1999). Spikes moved toward and away from the trough while the rat traveled toward or away from the place field center, respectively, resulting in an opposite phase relationship of the spikes, on average, for the rising (beginning-to-peak) and falling (peak-to-end) parts of the place field (Figure 1C; see below).

The distance between adjacent place field peaks of two neurons could be estimated from the temporal relationship of the corresponding neuronal spikes at two

different time scales. At the longer or "real-time scale," the time difference between the peaks of the smoothed cross-correlograms (CCG) corresponded to the time it took the rat to traverse the distance between place field peaks (Figures 1D and 1E). At the shorter or "theta time scale," the same distances were represented by the temporal relations of spikes at the tens of millisecond time scale (Figures 1F and 1G). Below, we refer to this distance versus theta-scale time-lag correlation as "sequence compression" and to its correlation coefficient as "sequence compression index."

Assembly Coding of Place Sequence Information

Sequence compression was suggested to be the direct consequence of the linear phase precession of individual neurons, relative to a global theta timing signal (Skaggs et al., 1996). It was also hypothesized that the phase of the spikes within the theta cycle but not their firing rate is the critical variable for place representation (Huxter et al., 2003). Because the pacemaker model does not assume direct interactions among the place cells, the most accurate prediction of the rat's position at any given place would be reflected by the phase-position correlation of the recorded multiple cells (Jensen and Lisman, 2000). Furthermore, the correlation between place field distances and the temporal differences of place cell spikes at the theta time scale would result exclusively from the theta phase precession. Alternatively, in the assembly model of place representation, the temporal differences between neuron pairs and the distances between corresponding place fields could reflect the strength of synaptic interactions between cell assemblies representing the two sequential positions (Muller et al., 1996). The two models predict identical phase precession slopes of individual place cells. However, the temporal correlation among assembly members and the encoding of spatial relations (distances) between their place fields should be better in the assembly model than in the pacemaker model because the former model assumes synaptic interactions among the neurons. To distinguish between these alternative mechanisms, we examined the transformation between real-time scale and theta-scale representations, the relationship between "dependent" and "independent" cell pairs, and spike time coordination during the rising and falling parts of the place fields.

To display the dynamics of ensemble representation of the corresponding spatial distances as the animal passed through sequential places, we plotted the sequence compression for the whole population of pairs (as in Figure 1G) over several theta cycles within a 1 s period. In Figure 2A, zero time-lag corresponds to the occurrence of spikes of the reference neurons averaged over multiple trials. The blue dots correspond to the averaged time-space occurrence of spikes of the paired neurons (Dragoi et al., 2003). This representation is analogous to simultaneously recording from every neuron in the hippocampus, each representing a single place field, and displaying the spatial-temporal evolution of the correlated ensemble spiking as the rat traverses the corresponding place field of a reference neuron. In Figure 2A, up to nine "clouds" can be recognized, spaced by 110–120 ms intervals, relating to the duration of theta oscillation. Spatial distances were repeatedly represented by the discharges of the partner neurons, beginning ~500 ms before the animal reached the center of the place and lasted for another 500 ms until the rat exited the field. The neuronal sequences were direction specific because distance versus time-lag plots of the same cell pairs poorly correlated on the opposite journey on the track (compare blue and black lines in Figure 2A). The accuracy of predicting the field center gradually increased in subsequent theta cycles as the animal approached it, as indicated by the strongest distance versus time correlation at the central cloud (Figure 2A). The spatial extent of the central cloud was ~40 cm, corresponding to the mean size of a place field in the dorsal hippocampus (Samsonovich and McNaughton, 1997). Because the average walking velocity of the rats on the track was 34 ± 0.21 cm/s, corresponding to ~5 cm per theta cycle, shifting parts of the same field were repeatedly and intermittently represented by the same groups of cells in six to nine subsequent theta cycles (Figure 2A). Because of the large size of the place fields, several place cells were active together in each theta cycle, but the group composition varied from cycle to cycle. The whole extent of the field was represented only once in the central cycle, surrounded by place cells of past and future positions. The similar sequence compression within the past and future clouds, as reflected by their similar axis orientation, is an indication of a relatively fixed temporal relationship among the active neurons. The real-time and theta-scale representations correlated at all distances (Figure 2B). The ratios between real-time and theta time scale representation of distances ("compression") increased with the length of the represented distance (Figure 2C), suggesting that the temporal coordination of neuronal discharges at the theta-scale improved as the animal approached the predicted place.

We addressed the stability of sequence compression by comparing runs in the first and last quarters of the sessions. Although each recording session was preceded by hours of activity in a different environment (i.e., home cage), sequence compression was present in the first quarter of laps and was not different from that of the last quarter (Figure 2D; $p = 0.3$, Z test for two correlation coefficients). This result suggests that once formed, the sequence compression emerges instantaneously in the proper spatial context.

Within sessions, individual place cells exhibited variable firing rates across different laps (Mehta et al., 1997; Fenton and Muller, 1998) (Figure 3A). We exploited this variability to contrast the predictions of the common pacemaker (independent phase-precession) versus coordinated assembly models. In principle, across-lap variability may occur independently within groups of neurons that separately encode nearby spatial positions and are most active on different laps (Samsonovich and McNaughton, 1997). Alternatively, spike activity may be temporally coordinated among sequentially active cell assemblies that bind adjacent locations into larger places on the linear track and whose discharges therefore covary within laps. To distinguish between these possibilities, cell pairs were separated on the basis of their lap-by-lap covariation of firing rates. Pairs with significant within-lap covariation of firing rates at the minute scale (corresponding to trial lengths) were

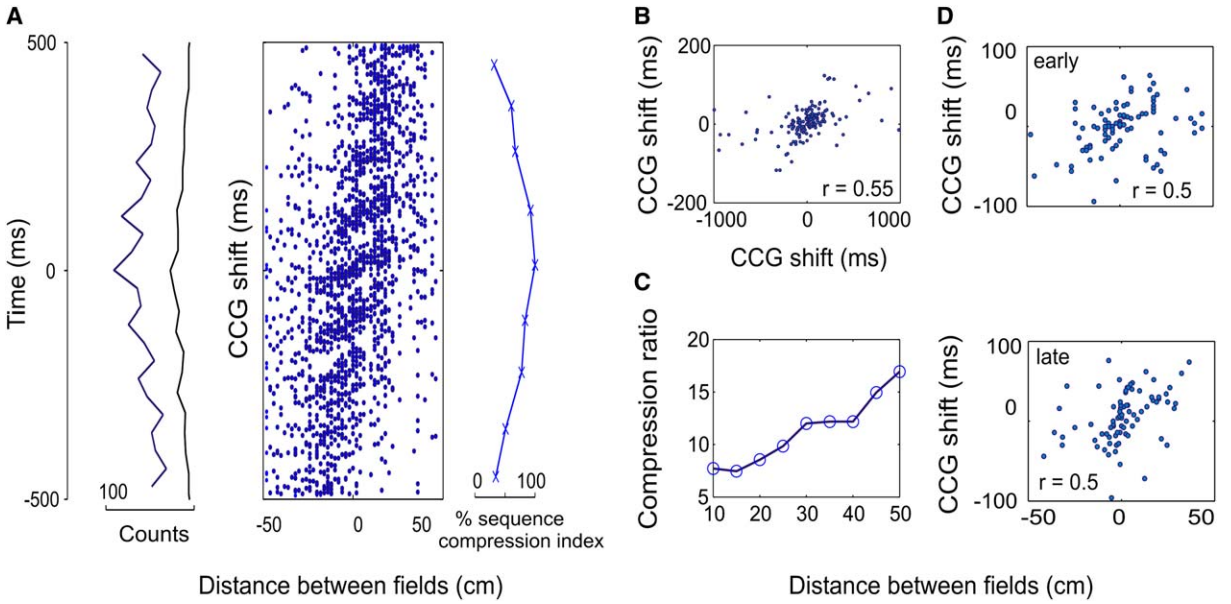

Figure 2. Repeated, Asymmetric, and Compressed Representation of Spatial Sequences by Populations of Place Cells

(A) Prospective (negative values) and retrospective (positive values) repeated encoding of spatial distances (box). Oscillatory (repetitive) asymmetric distribution of short time scale CCG peaks (left histograms), at ~9 Hz (blue line), and representation of distances by the same pairs (black line) recorded during runs in the opposite direction, demonstrating increased asymmetry of the internal representation. Dynamics of sequence compression indices across several cycles (right curve). Values on the x axis represent percentage of the sequence compression index at the central cloud (100%).

(B) Correlation between "real" (x axis) and theta time scale (y axis) CCG peaks of the same place cell pairs ("compression ratio").

(C) Magnitude of compression ratio is proportional with the encoded distance. Each data point was computed as the average compression ratio (y axis) of a subgroup of pairs that have their place field peaks separated by no more than the value displayed on the x axis. For each pair, compression ratio was calculated as the ratio between the temporal bias on the large time scale CCG and the temporal bias on the theta scale CCG.

(D) Sequence compression is present in the first quarter of the session (early) and is similar to the one in the end quarter of the session (late).

termed "dependent," whereas pairs with nonsignificant correlation were termed "independent" pairs. A pair was classified as dependent if its correlation coefficient, calculated over the whole session, was equal to or larger than the maximum of 500 times shuffled data of the same pair (mean r = 0.47 versus mean of the maximum shuffled correlation coefficient for each pair r = 0.33; $p = 10^{-11}$, paired t test) and independent when its correlation coefficient was smaller (Figure 3A). Eighty-one percent of the dependent pairs and 74% of the independent pairs were recorded from different electrodes. The sequence compression index (as calculated in Figure 1G and the central cloud in Figure 2A) in the dependent group (r = 0.82) was significantly larger than in the independent group (r = 0.51; Figures 3B and 3C, top; p = 0.0004; Z test for two correlation coefficients; Figure 3C, bottom; $p = 10^{-20}$, t test). Confining the analysis to dependent pairs recorded from separate electrodes did not affect the correlation values significantly (compare red and black lines in Figure 3C, top).

Although spatial proximity is a potential factor that favors binding of past, present, and future locations, it was not the primary cause of the observed increased correlation for the dependent group. Most of the dependent (90%) and independent (80%) pairs had their peaks separated by no more than 25 cm. For this critical, strongly overlapping range, the distance between place field peaks was similar among the dependent and independent groups (p = 0.073, Kolmogorov-Smirnov test). If spatial proximity were the single cause of sequence compression, one would expect no difference between the dependent and independent pairs with comparable distances. However, when the analysis was confined to these subgroups, the sequence compression index remained significantly higher in the dependent (r = 0.81) versus independent group (r = 0.55) (Figure 3C, top, compare blue and red lines, p = 0.004; Z test for two correlation coefficients).

To examine how well *individual* place cells from the dependent and independent groups predicted position by their firing rate or spike phase, we calculated the in-field peak rate and the correlation coefficient between position and phase of spikes for each neuron (we refer to this as "phase-position correlation"). The peak firing rates and the phase-position correlations were indistinguishable between the two groups (Figure 3D; p = 0.35 and p = 0.1, respectively, ranksum tests). Further control analyses excluded the contribution of four additional individual place cell features as the cause of the significantly larger sequence compression index in the dependent versus independent group. First, the fraction of spikes in burst (<6 ms interspike intervals) was comparable in the two groups (0.21 ± 0.01 versus 0.22 ± 0.01, p = 0.55, ranksum test). No difference was observed in the comparison of the place field lengths (Figure 3D; 50.3 ± 2.4 versus 54.9 ± 2.4 cm, p = 0.44, ranksum test) or the spatial distribution of place field peaks on the track (standard deviation: 71.1 versus 65.3 cm, p = 0.95, Kolmogorov-Smirnov test). In addition, the sequence compression index did not depend on the similarity in

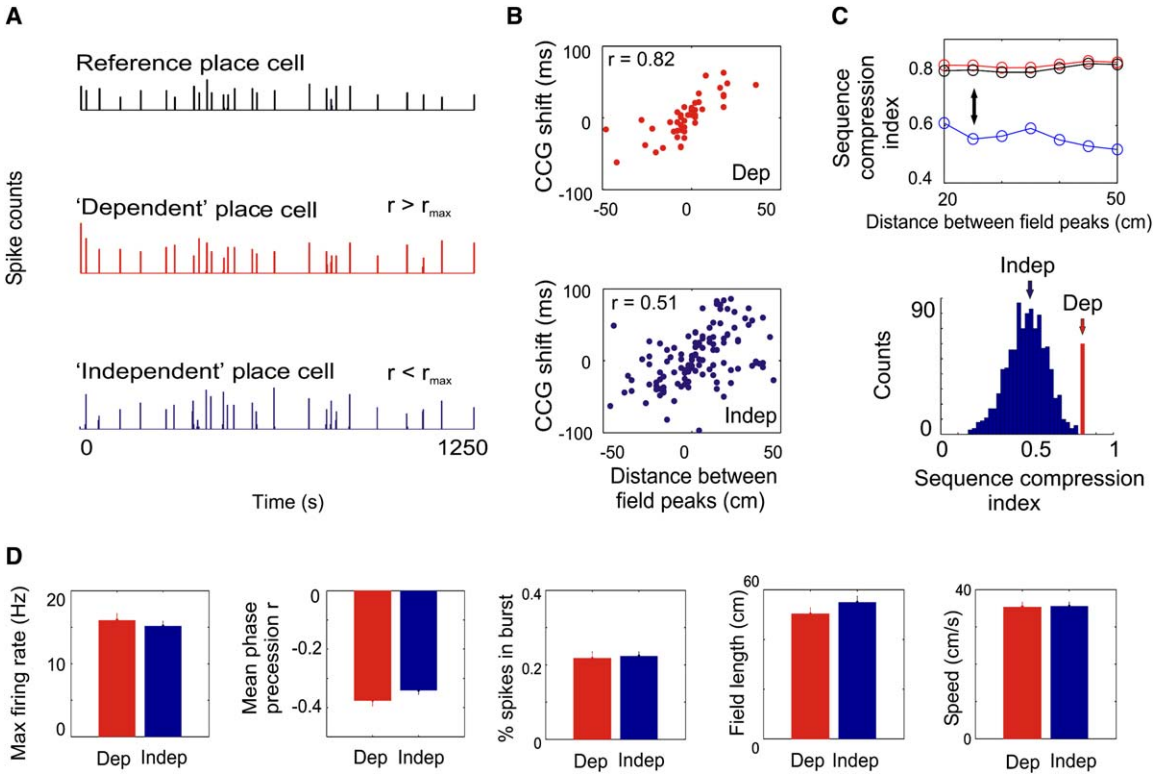

Figure 3. Place Sequences Are Best Represented by Temporal Coordination between Cell Assemblies

(A) Firing rates (counts per 2 s bins) of three place cells in a single session. The reference and "dependent" neuron (red) had a significant correlation of firing rates between laps (r), whereas the "independent" neuron (blue) did not (i.e., $r < r_{max}$). r_{max} = maximum value of the distribution of correlation coefficients between the reference and target cells after 1000 times random shuffling (see Experimental Procedures).

(B) Sequence compression (as in Figure 1G) for "dependent" (dep, red) and "independent" (indep, blue) pair of neurons.

(C) Tests of significance of temporal correlation among dependent (red) versus independent (blue) place cell pairs. (Top) Z test for two correlation coefficients applied to subgroups of data with similar distances between field peaks from the dependent (red) and independent (blue) groups. Arrow marks 25 cm distance between field peaks. In black are values for the dependent group after the elimination of cell pairs recorded by the same electrode. (Bottom) t test. Blue: the distribution of sequence compression indices for the independent pairs calculated repeatedly on a number of data points equal to the number of dependent pairs selected randomly (1000 iterations) from the larger population of independent pairs. Red: correlation value for the dependent pairs. The height of the red bar is magnified 60× for comparison.

(D) Individual cells of the "dependent" (red) and "independent" (blue) groups have similar in-field peak firing rates, phase-position correlation, percent of spikes in burst mode, place field length, and instantaneous speed of the animal while emitting spikes.

Bars are means and error bars are SEM.

slopes of phase precession, as the difference in slopes of dependent (median 2.68°/cm) and independent pair groups (median 2.01°/cm) were similar ($p = 0.59$, ranksum test). Finally, the instantaneous speed of the animal at which spikes were emitted by the included cells was also comparable for the two groups (Figure 3D; 35.25 ± 1.3 versus 35.57 ± 1 cm/s, $p = 0.78$, ranksum test), indicating that activity restricted to a particular area of the track or locations where the animal might have spent more time cannot account for the observed difference between the dependent and independent groups. Altogether, these results support the hypothesis that increased spatial-temporal correlation between dependent cell pairs is not caused by differences in individual place field features or by the animal's different motor behavior but rather by the enhanced temporal coordination among sequentially activated cells.

Firing rates of place cells increase in the rising part and decrease in the falling part of the field. It has been suggested that the linear nature of phase precession of place cell spikes through the entire theta cycle in multiple cells serves to disambiguate the relative position of the animal, in accordance with the common theta drive model (O'Keefe and Recce, 1993; Jensen and Lisman, 2000; Huxter et al., 2003). To compare and contrast the behavior of multiple independent single place cells with the hypothesized coordinated ensemble activity, we calculated the sequence compression index separately from spikes fired by pairs of cells in the rising or falling part of their fields. The sequence compression index was significantly higher during the rising ($r = 0.63$) than in the falling ($r = 0.3$) part (Figure 4A; $p = 0.0007$, Z test for two correlation coefficients). Accordingly, the theta-scale cross-correlograms between spikes fired by neuron pairs during the rising part of the place fields had significantly sharper peaks than those calculated from spikes fired in the falling part (Figure 4B; kurtosis excess for all pairs = −0.42 ± 0.05 and −0.77 ± 0.03, respectively; $p = 10^{-7}$, ranksum test). These findings suggest different degrees of temporal coordination in the two parts of the place field (roughly corresponding to the theta half-cycles, Figure 1C). Since the field theta

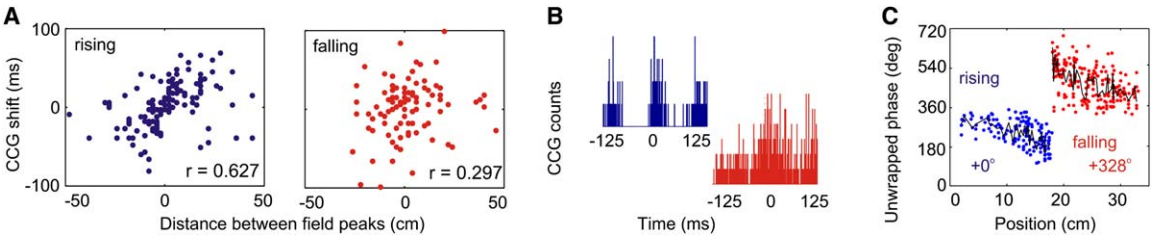

Figure 4. The Accuracy of Spatial Sequence Representation Is Different in the Rising and Falling Parts of the Place Field

(A) Sequence compression index for spikes emitted in the rising (blue) and falling (red) parts of the place field.

(B) Cross-correlograms (CCG) for a representative place cell pair in the rising (blue) versus falling (red) parts of the field. Note stronger modulation of the CCG in the rising part of the place field.

(C) Phase-position correlation plot for the rising (blue) and falling (red) parts of an example place field. Phase was "unwrapped" (O'Keefe and Recce, 1993) separately for each part of the field (values indicated under the data points) until the best position-unwrapped phase correlation was obtained. Black lines, running means for each part of the field.

oscillation remains the same while the rat crosses the entire field, these observations imply forces of coordination other than a common theta drive acting in the two parts of the field, consistent with the assembly/attractor model. On the other hand, several studies have shown that even in individual place cells, spike phase coupling is more reliable while the animal approaches the center of the place field compared to after it passed the field center (Skaggs et al., 1996; Mehta et al., 2002; Yamaguchi et al., 2002). Indeed, several parameters of single-cell activity were also different in the two parts. The phase-position correlation was significantly larger in the rising (−0.35 ± 0.009) than in the falling (−0.30 ± 0.008) part of the fields ($p = 10^{-4}$; ranksum test; an example is shown in Figure 4C). Consistent with this, phase variance was smaller in the rising versus falling part of the field (8571 ± 199 versus 9850 ± 182 deg^2, $p = 3 \times 10^{-6}$, paired t test; Figure 5A), while ordering and binning the data by position estimated a 24% (30.6° ± 3.5°, $p = 10^{-12}$, paired t test) increase in theta phase range (see Experimental Procedures) in the falling part of individual place fields. In addition, the fraction of spikes in bursts was significantly higher in the rising than in the falling part of the fields (0.23 ± 0.009 versus 0.17 ± 0.009; $p = 10^{-4}$, paired t test; Figure 5A). Neither the position variance (95.9 ± 15.7 versus 87.8 ± 11.6 cm^2, see Experimental Procedures) nor the position-phase slope (−4.81 ± 0.24 versus −4.48 ± 0.28°/cm) were different in the rising versus falling part of the fields (p = 0.67 and p = 0.94, respectively, paired t test; Figure 5A). According to the pacemaker model, the increased phase variability of independent single cells in the falling part of the place field accounts for the decreased sequence compression index. In contrast, the assembly model predicts that both the increased variability in single cells and the decreased sequence compression index reflect a decrease in spike coordination among the assembly members.

To examine whether the significant differences between the two parts of the field arise from a pacemaker mechanism only, we introduced temporal or phase jitter (see Experimental Procedures) to the spike times recorded during the rising part of the place fields to increase their variability (Figure 5B). Adding a 10 ms or 30° jitter to the spikes emitted in the rising part was sufficient to equalize the phase-position correlation (−0.29 ± 0.002, p = 0.3, t test), phase variance (9847 ± 35 deg^2, p = 0.98, t test), position-phase slope (−4.97 ± 0.04°/cm, p = 0.65, t test), and burst fraction (0.17 ± 0.004, p = 0.54, t test) with the values calculated from the original (nonjittered) spikes in the falling part of the fields (Figure 5B). Nevertheless, the sequence compression index calculated from the spikes after shuffling in the rising part remained significantly larger compared to the falling part of the place field (0.51 versus 0.30; $p = 10^{-200}$, t test; Figure 5B). Abolishing the difference in spike time coordination between the two parts of the field required a time jitter of at least 35 ms (78% above the observed variability) added to the spikes emitted in the rising part of the field (r = 0.296 versus r = 0.297; Figure 5B, left arrow; p > 0.6, t test). Importantly, the latter time jitter exceeded the physiologically estimated 10–30 ms long "lifetime" of the cell assemblies (Harris et al., 2003). Altogether, these observations indicate that temporal coordination of neurons and distance representation at theta time scale cannot be simply explained by a pacemaker drive of multiple independent phase-precessing cells but rather relies on precise timing among cell assemblies. To test this idea more directly, the cross-correlograms of the 10 ms jittered spikes from the rising part of the fields were compared with the cross-correlograms constructed from the original spike trains of cell pairs in the falling part of the fields. The jittered spikes maintained a significantly better temporal coordination (kurtosis excess = −0.69 ± 0.002, $p = 5 \times 10^{-7}$, ranksum test) than the spikes emitted in the falling part of the fields, despite similar phase-precession profiles. This suggests the existence of a transiently increased temporal correlation among and across assembly members that is more resistant to small perturbations in individual spike trains than their phase relationship to a global theta signal, representing a more robust way of preserving sequences.

Cooperation of CA3 and CA1 Assemblies

Recent studies have emphasized the distinct functional roles of CA3 and CA1 neurons (Leutgeb et al., 2004; Lee et al., 2004a, 2004b). Our findings add further support for the functional differences between these regions and explore their interactions within theta cycle. CA3 place fields were more often bidirectional than CA1 neurons, as measured by the median distance between the place

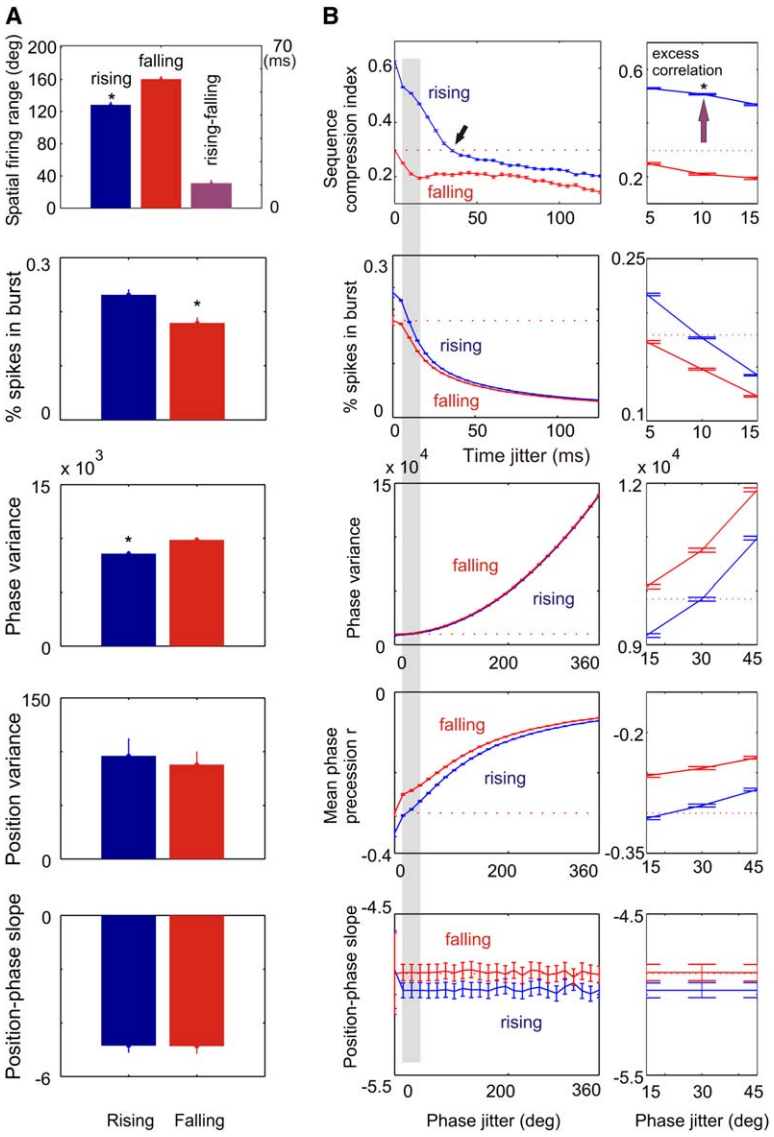

Figure 5. Comparison of Individual Cell and Cell-Pair Features in the Rising and Falling Parts of the Place Field without (Original) and with Spike Time/Phase Jitter

(A) Original spike trains. Blue, rising part; red, falling part of the place field. From top to bottom, averages of phase ranges, burst fraction, phase variance, spike position variance, and place-phase slope. Purple: mean of the paired falling minus rising part differences in phase ranges. Scale on the right y axis is in milliseconds (for 8 Hz theta). Bars are means and error bars are SEM.

(B) Changes in individual cell and cell-pair features as a function of jittered spike times/phases (x axis: 5 ms or 30° steps). Blue, rising part; red, falling part of the place field. (Left) From top to bottom (mean ± SEM): sequence compression index, burst fraction, phase variance, position-phase correlation, and slope of phase-place plot. Red dotted line: nonjittered value for the falling part of the field. Arrow: adding 35 ms jitter to spikes in the rising part of the fields reduced the sequence compression index to that of the nonjittered spikes emitted in the falling part of the field. Gray rectangle, critical time/phase window within which jittered activity in the rising part of the fields becomes similar to the original spike trains in the falling part of the fields. (Right panels) Higher-resolution view of the critical time window. Arrow, "excess" sequence compression index.

field peaks while the rat was running in clockwise and counterclockwise directions (Figure 6A; 37 ± 3.7 cm for CA1, 16 ± 4.8 cm for CA3 neurons; $p = 0.015$, ranksum test). Moreover, the firing rates of place cells in the two directions of movement were significantly more correlated for the CA3 ($r = 0.58$) than the CA1 ($r = 0.35$) place cells ($p = 0.02$; Z test for two correlation coefficients). The phase-position correlation was significantly smaller for the falling part of the field in CA1 pyramidal cells, compared to the rising part ($r = -0.32$ versus $r = -0.37$; $p = 10^{-4}$, ranksum test) and comparable to the correlation coefficients of CA3 neurons in both parts of the field (Figure 6B; $r = -0.28$ versus $r = -0.31$; $p = 0.54$, ranksum test). This pattern of results was not altered when, for each cell, spike phases were referenced to the locally recorded theta signal (in the CA3 or CA1 pyramidal layer) rather than CA1 pyramidal layer (CA1 theta versus local theta: $p > 0.44$, paired t tests). Whereas the firing rates of CA1 pyramidal cells were comparable in the two parts of the field, CA3 neurons were more active in the rising than falling half of the place field (CA3 skewness = −0.14 ± 0.04 versus −0.04 ± 0.03 in CA1; $p = 0.003$, ranksum test; Figure 6C). The increased negative skewness (see also Lee et al., 2004a) and reduced directionality of CA3 versus CA1 neurons suggest that direction of movement and sequential order are specified in a different manner within the two populations of pyramidal cells.

Differences between the two parts of the place field presented above are further supported by the theta scale temporal relationship of CA1 and CA3 pyramidal cells. The two principal cell populations preferentially fired on opposite phases of the theta oscillation in both the rising and falling parts of the place field (Figure 6D). This result suggests that CA3 assemblies predicted the current location of the animal about one-half theta cycle earlier than the CA1 representation and implies that different processes take place across different phases of the theta oscillation (Hasselmo et al., 2002). Despite these differences, spatial distances were represented within and across hippocampal regions by the theta scale temporal lags between CA3-CA3 (15% of all pairs),

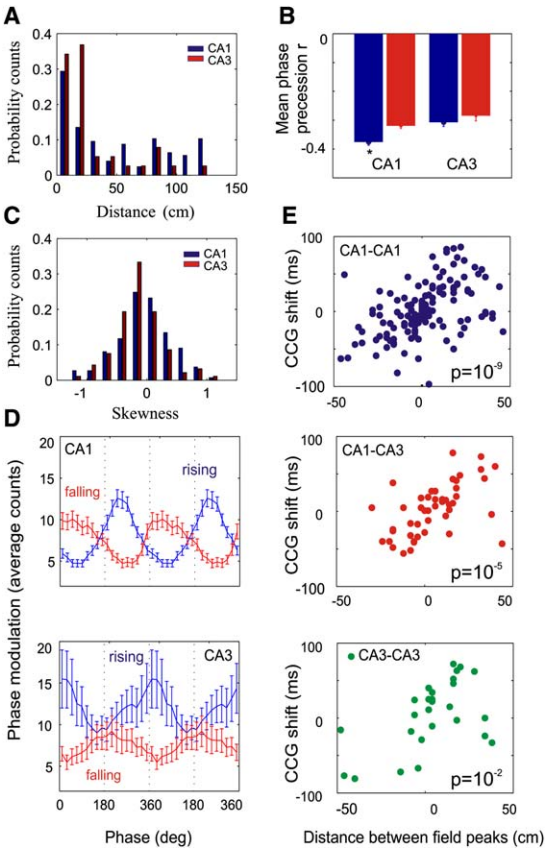

Figure 6. Different Computations in the CA1 and CA3 Regions

(A) Directionality measure, defined as distance between place field peaks of the same cell while the rat is running in clockwise versus counterclockwise directions (normalized). Note reduced directionality of CA3 fields (red) compared to CA1 (blue).

(B) Phase-position correlations for the rising (blue) and falling (red) parts of the place fields for CA1 and CA3 cells (mean ± SEM.). *, significant difference between the two parts ($p = 10^{-4}$, ranksum test).

(C) Increased negative skewness of CA3 (red) versus CA1 (blue) place fields (normalized).

(D) Phase of unit discharge of place cell spikes for the rising (blue) and falling (red) parts of the field for CA1 (left) and CA3 (right) place cells (reference: CA1 pyramidal layer theta). Note nearly opposite phase preference of CA1 and CA3 place cells in both parts of the field. Error bars are SEM.

(E) Sequence compression index for neuron pairs within and across hippocampal subfields.

CA3-CA1 (23%), and CA1-CA1 place cell pairs, as indicated by the significant sequence compression indices in each comparison (Figure 6E).

The peaks of the unit autocorrelograms allowed us to compare the frequency of the oscillating action potential trains across regions and with the field theta rhythm (O'Keefe and Recce, 1993). The frequency of place cell oscillation of both CA1 and CA3 place cells (9.77 ± 0.12 Hz and 10.51 ± 0.28 Hz) was significantly faster than the mean theta frequency in the CA1 pyramidal layer (O'Keefe and Recce, 1993) (7.93 ± 0.15 Hz; $p = 5 \times 10^{-6}$ and $p = 10^{-6}$, respectively, ranksum test). The frequency of spike oscillations of both CA1 and CA3 neurons were comparable in the rising and falling parts of the place field (CA1 cells [n = 123]: 9.78 ± 0.15 Hz and 9.76 ± 0.23 Hz, respectively; CA3 [n = 44 cells]: 10.52 ± 0.34 Hz and 10.06 ± 0.43 Hz, respectively). Nevertheless, analysis of variance revealed a significant group effect (CA3 faster than CA1, p = 0.004), and a post hoc comparison indicated that this difference was due to the higher-frequency oscillatory activity of CA3 neurons in the first half of place fields (p = 0.016, ranksum test).

Discussion

Our findings suggest that sequential but phase-shifted activation of CA3 and CA1 cell assemblies in the hippocampus can maintain past information, identify a current item, predict future ones, and bind them into a sequence. We hypothesize that the sequences are stored in the autoassociative CA3 recurrent and CA3-CA1 collateral systems (Muller et al., 1996; Jensen and Lisman, 1996; Tsodyks, 1999) and are updated by entorhinal cortex-mediated environmental signals (Zugaro et al., 2005; Hafting et al., 2005) according to the following scenario (Figure 7). During each theta cycle, the CA3-CA1 synaptic space is searched, recalling several temporally linked cell assemblies, each representing spatial fields that the rat just passed and would traverse during the next second or so. Therefore, this compression mechanism provides a spatial-temporal context for the current item represented by the most active assembly. The internal sequence readout in the CA3 autoassociator (Kanerva, 1988; Treves and Rolls, 1992) is triggered by the environmental input of the previous locations by way of the entorhinal cortex (Frank et al., 2000; Hafting et al., 2005). The readout is forward in time, reflecting the sequence order during learning. The receptive fields of the cell assemblies are ~40 cm in size and shifted by 4–5 cm, corresponding to the distance moved by the rat in a single theta cycle (Samsonovich and McNaughton, 1997). The predicted and perceived locations are replayed in tandem by the CA3 and CA1 assemblies. The asymmetric nature of spike timing-dependent plasticity (Levy and Steward, 1979; Markram et al., 1997; Magee and Johnston, 1997; Bi and Poo, 1999) favors temporally forward associations in sequentially active assemblies (Mehta et al., 1997). A consequence of the oscillatory temporal organization of cell assemblies is the theta phase precession of spikes of single place cells. We suggest that the overlapping past, present, and future locations are combined into single episodes by sequential CA3 and CA1 assemblies in successive theta cycles. Several computational models and empirical observations are compatible with the above scenario (Hebb, 1949; Levy and Steward, 1979; Lisman and Idiart, 1995; Muller et al., 1996; Jensen and Lisman, 1996; Mehta et al., 1997; Wallenstein and Hasselmo, 1997; Samsonovich and McNaughton, 1997; Tsodyks, 1999; Nakazawa et al., 2002; Brun et al., 2002; Hasselmo et al., 2002; Zugaro et al., 2005).

Temporal Coordination of Position Sequences

The distances between place field centers could be deduced from both the peak firing rates of neuron pairs on the track and their temporal differences at theta time scale. During successive theta cycles, multiple neurons, representing overlapping place fields, shifted together and sustained a temporal order relationship with each

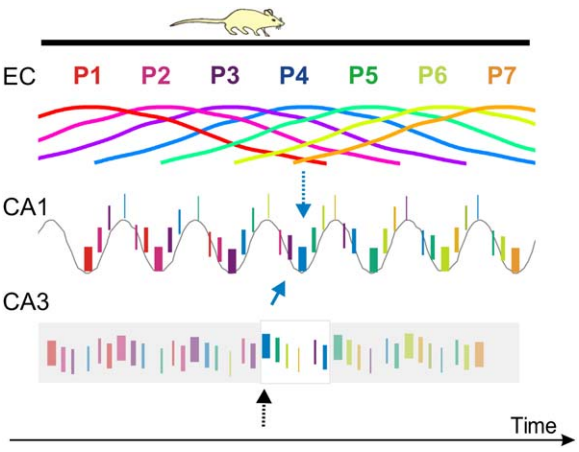

Figure 7. Illustration of the Spatial-Temporal Context and the Interactions among CA3 and CA1 Cell Assemblies

Each position (P1 to P7) is defined by the most active cell assembly firing at the trough of the theta cycle (e.g., P4 by the blue assembly). The width of the bars indicates firing rates of the hypothesized assemblies while the theta time scale temporal differences between assemblies reflect distances of their spatial representations. Because each assembly contributes to multiple place representations, multiple assemblies are coactivated in each theta cycle. As a result, the current position/item, represented by the maximally active assembly at the cycle trough, is embedded in the temporal context of past and future representations. Assembly sequences within theta cycles could reflect strengthening of connections not only between adjacent places/items (e.g., P4-P5) but also between nonadjacent (e.g., P3-P5; P4-P6) items. This mechanism may allow distances to be translated into time and time into synaptic weights. The CA3 and CA1 representations correspond to the predicted (blue solid arrow) and updated positions (blue dotted arrow) by the entorhinal cortex (EC), respectively. One position is indicated by the boxed area. In the CA3 recurrent system, the temporal differences among assembly members are assumed to be reflecting synaptic strengths between assembly members. Black dotted arrow: hypothesized initiation of sequence recall.

other so that the cell that fired on the earliest phase represented a place field whose center the rat visited first. This sequence compression was suggested to be the consequence of spike phase precession of individual neurons, relative to a global theta timing signal (Skaggs et al., 1996). In the simplest case, pyramidal neurons are paced by the interference of two harmonic oscillators with a small period offset, such as the medial septal "pacemaker" input and the entorhinal input (O'Keefe and Recce, 1993). However, without additional mechanisms, the phase interference model cannot explain the phase-shifted sequences of CA3 and CA1 neurons described here or the field size-determined differential slopes of individual place cells. A refined version of the dual-oscillator model operates at a single-cell level. In this case, a transient dendritic depolarization from spatial inputs produces a voltage-dependent oscillation at a frequency slightly faster than the somatic pacemaker theta input (Kamondi et al., 1998; Mehta et al., 2002; Harris et al., 2002). Because neurons with stronger spatial inputs oscillate faster, they have steeper phase precession slopes and smaller place fields. If place cells are sequentially activated on the track, a direct consequence of the single-cell model of spike phase precession is the theta time scale temporal correlation between neuron pairs with overlapping place fields. However, because the pacemaker interference models do not assume direct interactions among the place cells, the "ideal" phase precession slope for a single place neuron in any given trial would be that of the average slope across all trials. According to this model, the correlation between distances of place fields and the time/phase differences of place neurons at the theta time scale should arise from externally regulated timing mechanisms (Jensen and Lisman, 2000).

Our findings showed a significantly better temporal coordination among place cells than predicted by the phase interference pacemaker models. This is not surprising, because hippocampal neurons are embedded in an interactive synaptic environment, and the timing of their action potentials is biased not only by theta oscillation pacing but also by all their synaptically connected and spiking peers (Harris et al., 2003). The great majority of intrahippocampal synapses is established by the collateral system of CA3 neurons (Amaral and Witter, 1989; Li et al., 1994), and it has been hypothesized that distances between place fields are encoded in the synaptic strengths between CA3-CA3 and CA3-CA1 neuron pairs (Muller et al., 1996). The excess temporal correlations, therefore, may be explained by the experience-dependent modification of synaptic strengths during the initial exploration of the maze.

Our alternative hypothesis for the theta time scale correlation among neurons is that sequential positions on the track are represented by unique sets of cell assemblies, and phase precession of spikes is a result of temporally coordinated activity within and between anatomically distributed groups of sequentially activated cell assemblies. A key mechanism in this process is the ability of the CA3 collateral system to support theta oscillation (Konopacki et al., 1988; Fisahn et al., 1998; Kocsis et al., 1999). While the rat is traversing the track, unique combinations of pyramidal cells are active in successive theta cycles. The most active group at the trough of the theta cycle (in the CA1 pyramidal layer) defines the current location, flanked by spikes of other neurons on the descending and ascending phases of theta, representing past and future locations, respectively. We hypothesize that as the rat moves forward, neurons on the ascending phase are attracted to the trough to represent a new location because the oscillating assembly representing the current position exerts an excitation on the trailing groups of neurons and advances their phase (Williams et al., 1990). The synaptic strengths among member neurons of an assembly, representing the same location and discharging within the same gamma cycle (Lisman and Idiart, 1995; Harris et al., 2003), determines the place field size and, consequently, the slope of the spike phase precession of the participating member neurons. Synaptic strengths across assemblies, representing different locations and discharging in different gamma cycles, can determine both their time/phase differences within the theta cycle and the distances between the respective place fields. In addition, the oscillating assemblies may also be responsible for the temporal coordination of medial septal neurons by way of the hippocampo-septally projecting inhibitory interneurons (Dragoi et al., 1999; Wang, 2002; Gulyas et al.,

2003). The self-organized assembly model is supported by the empirical observation that the learned neuronal sequences of place fields are spontaneously replayed during immobility and sleep-related sharp wave bursts (Wilson and McNaughton, 1994; Nadasdy et al., 1999; Lee and Wilson, 2002) without extrahippocampal influences at a time scale slightly faster than during a given theta cycle. The sharp wave-related activity may represent a mechanism for stabilization of assembly sequences (Buzsaki, 1989; Samsonovich and Ascoli, 2005). The observation that artificial plastic alteration of intrahippocampal connectivity can modify previously learned neuronal sequences of place fields (Dragoi et al., 2003) provides further support for the assembly model. However, the internally coordinated assembly model alone cannot account for the phase-shifted activity of CA3 and CA1 cell assemblies.

Complementary Representation of Place Sequences in CA1 and CA3 Regions

In the behaving animal, the concurrently active CA3 place cells are an important source of the intrahippocampal theta and gamma rhythms (Kocsis et al., 1999; Csicsvari et al., 2003). The excitatory CA3 recurrent collaterals activate and coordinate interneurons in both the CA3 and CA1 regions, building up temporally covarying inhibition and gamma power nested within the theta cycles (Csicsvari et al., 2003). Maximum inhibition and gamma frequency power occur simultaneously in the two regions, but coupled to the opposite phases of the respective local theta cycles. As a result, CA1 neurons can discharge maximally when their perisomatic inhibition is weakest, likely activated by the direct entorhinal input (Brun et al., 2002). The CA3 input can assist in this process by at least two different ways. First, the CA3 generated feedforward inhibition can facilitate rebound discharges of CA1 place cells (Cobb et al., 1995). Second, CA3 afferents can convert the dominant feedforward inhibition of the entorhinal input to excitation. In vitro experiments showed that electrical stimulation of the entorhinal input typically evokes hyperpolarization in CA1 pyramidal cells. However, when the entorhinal input is activated 40–60 ms (i.e., half of the theta cycle) after stimulating the CA3 afferents, the hyperpolarization was converted into depolarization and discharge of the cell, due to a transient activation of NMDA receptors and decreased release of GABA from the inhibitory terminals (Ang et al., 2005).

The systems implication of the above findings is that the most active CA3 assembly in a given theta cycle represents the predicted location of the rat's head in the next half of the theta cycle. If the layer 3 entorhinal input, mediating the environmental effects (Hafting et al., 2005), "matches" the internal prediction, the CA1 pyramidal cells will respond. However, if the prediction is not confirmed, the entorhinal input remains ineffective. By temporally interleaving the entorhinal cortex-mediated input with the CA3-generated assembly sequences, the discharging CA1 pyramidal cells can provide an update of position information in each theta cycle (Zugaro et al., 2005). Viewed from this perspective, the CA3 and CA1 systems operate as a functional unit during theta oscillation.

Theta Cycle Compression of Sequences and Episodic Memory

An interesting and challenging question in hippocampal research is how a given physiological mechanism that evolved in a small-brain animal (e.g., navigation in physical space) can be employed for more complex tasks in humans (e.g., memory storage and retrieval). A route passed by the rat in a simple maze can be tracked by calculating the distances between cues, using self-generated signals and time by a mechanism referred to as dead reckoning or path integration navigation (McNaughton et al., 1996). There are many parallels between path integration and episodic memory (Buzsaki, 2005). First, return to the home base by path integration is possible after a single exploration. Similarly, episodic learning usually requires a single trial. Second, both path integration and episodic memory are self-referenced and both require a spatio-temporal context (Tulving, 1972; Squire, 1992). Third, both processes rely on sequential information, primarily on the temporal relationship between successive items. Fourth, in episodic learning, stronger associations are formed between stimuli that occur near each other in time, compared to those that are separated by a greater interval, although temporal links are established in both cases. Finally, in learning, forward serial associations are stronger than backward associations (Tulving, 1969; Kahana, 1996; Fortin et al., 2004; Howard et al., 2005). The neuronal firing patterns observed physiologically in the rat hippocampus could account for these behavioral observations in humans. The temporal relationship between neuron pairs was dramatically different in the opposite directions of locomotion (McNaughton et al., 1983). The position sequences in the maze were compressed into single theta cycles, i.e., within the time window of spike timing-dependent plasticity. The temporally compressed representation of distances can facilitate the association of not only immediately adjacent positions but also integrates nonadjacent ones (higher-order relations) because what matters for the strengthening of synapses is the temporal interval between the spikes in the pre- and postsynaptic neurons (Levy and Steward, 1979). Testing of free recall of the learned episodes in rats is difficult because the animals are exposed to the same environment in repeated trials. Nevertheless, the time compression of spikes into single theta cycles and the phase shifts of cells assemblies in the CA3 and CA1 regions indicate that hippocampal neurons do not simply represent the sensory environment, but generate sequence information required for both path integration and episodic memory.

Experimental Procedures

Four male Sprague-Dawley rats were implanted with eight independently movable tetrodes in the dorsal hippocampus. Surgery, recording, behavioral training, and unit separation were as described earlier (Dragoi et al., 2003). A total of 391 place fields in both directions were analyzed in this study, 298 fields from 193 CA1 place cells and 93 from 63 CA3 cells.

Theta Phase Analyses

The theta phase of unit firing was determined by a Hilbert transform (Harris et al., 2003), after filtering the EEG in the theta range (6–10 Hz). The phase preference of unit discharge for rising/falling parts

of the field of place cells was calculated using a unique reference theta EEG signal recorded from the CA1 pyramidal layer as confirmed histologically and physiologically by the presence of many active pyramidal cells and large-amplitude ripples at rest. Phase histograms were constructed for each cell using 20º bins, and the significant histograms ($p < 0.005$, Rayleigh test) were averaged, and mean and standard errors were calculated for each bin. Phase-position correlations and slopes were calculated using circular statistics (O'Keefe and Recce, 1993; Huxter et al., 2003) on at least 100 data points (50 for half-fields). For each place cell and for the whole session, the position of the spikes was plotted against their phase, separately for the rising and falling part of the field after maximizing the corresponding phase-position correlation considering the circular nature of the phase (see Figure 4C). From the beginning to peak and peak to end of the place field, a phase range was calculated for each nonoverlapping subgroup of four consecutive data points (bin size = four points). The median of the distribution of phase ranges, calculated for the rising versus falling part of the field for each cell, was used further for comparison. The spatial size of each bin was similar for the inbound and outbound portions of the field (0.31 ± 0.02 cm inbound and 0.34 ± 0.02 cm outbound; $p = 0.3$, paired t test). Phase variance and position versus phase slopes (slope of the least-squares linear regression line) were calculated after maximizing the corresponding phase-position correlation, considering the circular nature of phase. Spike position variance was calculated as the variance of the distribution of on-track spatial positions (distance in centimeters from the beginning of the track) corresponding to the emitted spikes. For computing the average theta frequency, theta oscillation epochs were detected (Dragoi et al., 2003), power spectrum was calculated for the entire session, and the local frequency maximum in the theta range (6–10 Hz) was detected.

Cross-Correlation and Sequence Compression Analyses

"Real-time" scale cross-correlograms (CCGs) between cell pairs were calculated in 3 s windows with 3 ms bin size. The single peak on the CCG was detected after low-pass filtering below 1.5 Hz. The theta time scale CCGs were calculated in 350 ms or 1 s (Figure 2A) windows, with 1 ms bin size. Fast CCG peaks were detected in 50 ms windows after filtering below 40 Hz. CCGs with <1 count/ms or with no significant peak (< mean + 1.5 SD for CA1-CA1 and CA3-CA1 pairs; +1 SD for CA3-CA3 pairs; +0.5 SD for rising/falling parts of the field and for first/last quarters of sessions) were discarded. Autocorrelograms (ACGs) were calculated as described above for the CCGs in 1 s windows. The time lag between the two largest peaks (low pass 40 Hz) was calculated and converted into frequency to compute place cell oscillation frequency. Distances between any two locations were calculated as the difference between the positions of the peaks of the two place fields, defined by the maximum firing rates. Both the spatial distance versus CCG time-lag correlations (sequence compression indices) and the position-phase correlation coefficients were calculated using Spearman's rank correlation. Sessions were divided into quarters by laps. The average number of laps in each direction was 32.5.

Dependent/Independent Pairs Analyses

For the detection of "dependent" pairs, spike times of each cell were binned at 2 s such that the entire rate activity on a lap was compressed in one bin (or occasionally two adjacent bins). After excluding the common zero-value bins, for all cell pairs, a correlation coefficient was calculated between the binned activities of the pair members. This measure reflected the degree of coactivation of neuron pairs on multiple trials and was thus independent from the fine temporal analysis of the CCG. The correlation coefficient was subsequently compared with a distribution of correlation values obtained by time shuffling the nonzero bins of one member of the pair 500 times. The criterion of "dependent pair" was met for each individual pair when the data-based correlation coefficient was larger or equal than the maximum of the distribution of shuffled values for that pair. The use of a qualitative criterion for pair separation leading to noncontinuous variables was imposed by the fact that sequence compression index reflects a group value while dependence/independence (coordination index) is calculated for each pair of neurons. Computing a one-to-one correlation between sequence compression and dependence as a continuous variable was thus not possible. Using the criterion of absolute value of the lap-by-lap correlation coefficient to arbitrarily create several groups of cell pairs indicated the possibility of a nonlinear relationship between correlation coefficients and sequence compression index. Because the number of dependent pairs was smaller than that of independent pairs, the value of the sequence compression index for the dependent pairs (one value for the whole group of pairs) was compared (t test) with a population (distribution) of indices created using an equal number of data points with the dependent group selected randomly (1000 iterations) from the larger population of independent pairs (Figure 3C, bottom). Skewness was calculated as the ratio between the third central moment and the cube of the standard deviation. Kurtosis was calculated as the ratio between the fourth central moment and the fourth power of the standard deviation. Kurtosis excess is generally a measure of "peakedness" of a distribution. In our case, the closest to zero "cycle" of the oscillatory theta scale CCG (see Figure 1F) was treated as a distribution whose kurtosis excess value measured how sharp/precise the CCG/temporal coordination was. The length of place field was generally defined as the distance (in centimeters) between the two borders of the place field (places where the rate was more than 10% of the peak firing rate). Burst events were defined as spikes emitted within 6 ms interspike intervals. Instantaneous velocity of the animal was determined separately for each place cell, by dividing the length of its field by the time it took the animal to traverse it.

Time/Phase Jitter Analyses

The time (phase) jitter of spikes was performed by adding to the original spike time epochs (phases)—for each spike time (phase) individually—of a value extracted from a random normal population of time intervals (phase values) with mean zero and standard deviation equal with the value of the time (phase) jitter. The procedure was repeated 500 times for each value of the jitter: 5–125 ms in 5 ms increments (time), or 15º to 360º in 15º increments (phase).

Acknowledgments

We thank S. Tonegawa for his support and discussions; and M.A. Wilson for discussions. We also thank N. Kopell and J.E. Lisman for comments on an earlier version of the manuscript; and D. Nguyen for technical advice. Supported by grants from the NIH. The authors declare that they have no competing financial interest.

Received: November 3, 2005
Revised: January 3, 2006
Accepted: February 16, 2006
Published: April 5, 2006

References

Amaral, D.G., and Witter, M.P. (1989). The three-dimensional organization of the hippocampal formation: a review of anatomical data. Neuroscience *31*, 571–591.

Ang, C.W., Carlson, G.C., and Coulter, D.A. (2005). Hippocampal CA1 circuitry dynamically gates direct cortical inputs preferentially at theta frequencies. J. Neurosci. *25*, 9567–9580.

Bi, G., and Poo, M. (1999). Distributed synaptic modification in neural networks induced by patterned stimulation. Nature *401*, 792–796.

Brun, V.H., Otnass, M.K., Molden, S., Steffenach, H.A., Witter, M.P., Moser, M.B., and Moser, E.I. (2002). Place cells and place recognition maintained by direct entorhinal-hippocampal circuitry. Science *296*, 2243–2246.

Buzsaki, G. (1989). Two-stage model of memory trace formation: a role for "noisy" brain states. Neuroscience *31*, 551–570.

Buzsaki, G. (2005). Theta rhythm of navigation: link between path integration and landmark navigation, episodic and semantic memory. Hippocampus *15*, 827–840.

Cobb, S.R., Buhl, E.H., Halasy, K., Paulsen, O., and Somogyi, P. (1995). Synchronization of neuronal activity in hippocampus by individual GABAergic interneurons. Nature *378*, 75–78.

Csicsvari, J., Jamieson, B., Wise, K.D., and Buzsaki, G. (2003). Mechanisms of gamma oscillations in the hippocampus of the behaving rat. Neuron *37*, 311–322.

Dragoi, G., Carpi, D., Recce, M., Csicsvari, J., and Buzsaki, G. (1999). Interactions between hippocampus and medial septum during sharp waves and theta oscillation in the behaving rat. J. Neurosci. *19*, 6191–6199.

Dragoi, G., Harris, K.D., and Buzsaki, G. (2003). Place representation within hippocampal networks is modified by long-term potentiation. Neuron *39*, 843–853.

Eichenbaum, H., Dudchenko, P., Wood, E., Shapiro, M., and Tanila, H. (1999). The hippocampus, memory, and place cells: is it spatial memory or a memory space? Neuron *23*, 209–226.

Fenton, A.A., and Muller, R.U. (1998). Place cell discharge is extremely variable during individual passes of the rat through the firing field. Proc. Natl. Acad. Sci. USA *95*, 3182–3187.

Fisahn, A., Pike, F.G., Buhl, E.H., and Paulsen, O. (1998). Cholinergic induction of network oscillations at 40 Hz in the hippocampus in vitro. Nature *394*, 186–189.

Fortin, N.J., Wright, S.P., and Eichenbaum, H. (2004). Recollection-like memory retrieval in rats is dependent on the hippocampus. Nature *431*, 188–191.

Frank, L.M., Brown, E.N., and Wilson, M. (2000). Trajectory encoding in the hippocampus and entorhinal cortex. Neuron *27*, 169–178.

Gulyas, A.I., Hajos, N., Katona, I., and Freund, T.F. (2003). Interneurons are the local targets of hippocampal inhibitory cells which project to the medial septum. Eur. J. Neurosci. *17*, 1861–1872.

Hafting, T., Fyhn, M., Molden, S., Moser, M.B., and Moser, E.I. (2005). Microstructure of a spatial map in the entorhinal cortex. Nature *436*, 801–806.

Harris, K.D., Henze, D.A., Hirase, H., Leinekugel, X., Dragoi, G., Czurko, A., and Buzsaki, G. (2002). Spike train dynamics predicts theta-related phase precession in hippocampal pyramidal cells. Nature *417*, 738–741.

Harris, K.D., Csicsvari, J., Hirase, H., Dragoi, G., and Buzsaki, G. (2003). Organization of cell assemblies in the hippocampus. Nature *424*, 552–556.

Hasselmo, M.E., Bodelon, C., and Wyble, B.P. (2002). A proposed function for hippocampal theta rhythm: separate phases of encoding and retrieval enhance reversal of prior learning. Neural Comput. *14*, 793–817.

Hebb, D.O. (1949). The Organization of Behavior: A Neuropsychological Theory (New York: Wiley).

Howard, M.W., Fotedar, M.S., Datey, A.V., and Hasselmo, M.E. (2005). The temporal context model in spatial navigation and relational learning: toward a common explanation of medial temporal lobe function across domains. Psychol. Rev. *112*, 75–116.

Huxter, J., Burgess, N., and O'Keefe, J. (2003). Independent rate and temporal coding in hippocampal pyramidal cells. Nature *425*, 828–832.

Jensen, O., and Lisman, J.E. (2000). Position reconstruction from an ensemble of hippocampal place cells: contribution of theta phase coding. J. Neurophysiol. *83*, 2602–2609.

Jensen, O., and Lisman, J.E. (1996). Hippocampal CA3 region predicts memory sequences: accounting for the phase precession of place cells. Learn. Mem. *3*, 279–287.

Kahana, M.J. (1996). Associative retrieval processes in free recall. Mem. Cognit. *24*, 103–109.

Kamondi, A., Acsady, L., Wang, X.J., and Buzsaki, G. (1998). Theta oscillations in somata and dendrites of hippocampal pyramidal cells in vivo: activity-dependent phase-precession of action potentials. Hippocampus *8*, 244–261.

Kanerva, P. (1988). Sparse Distributed Memory (Cambridge, MA: MIT Press).

Kocsis, B., Bragin, A., and Buzsaki, G. (1999). Interdependence of multiple theta generators in the hippocampus: a partial coherence analysis. J. Neurosci. *19*, 6200–6212.

Konopacki, J., Bland, B.H., and Roth, S.H. (1988). Carbachol-induced EEG 'theta' in hippocampal formation slices: evidence for a third generator of theta in CA3c area. Brain Res. *451*, 33–42.

Lee, A.K., and Wilson, M.A. (2002). Memory of sequential experience in the hippocampus during slow wave sleep. Neuron *36*, 1183–1194.

Lee, I., Rao, G., and Knierim, J.J. (2004a). A double dissociation between hippocampal subfields: differential time course of CA3 and CA1 place cells for processing changed environments. Neuron *42*, 803–815.

Lee, I., Yoganarasimha, D., Rao, G., and Knierim, J.J. (2004b). Comparison of population coherence of place cells in hippocampal subfields CA1 and CA3. Nature *430*, 456–459.

Leutgeb, S., Leutgeb, J.K., Treves, A., Moser, M.B., and Moser, E.I. (2004). Distinct ensemble codes in hippocampal areas CA3 and CA1. Science *305*, 1295–1298.

Levy, W.B., and Steward, O. (1979). Synapses as associative memory elements in the hippocampal formation. Brain Res. *175*, 233–245.

Li, X.G., Somogyi, P., Ylinen, A., and Buzsaki, G. (1994). The hippocampal CA3 network: an in vivo intracellular labeling study. J. Comp. Neurol. *339*, 181–208.

Lisman, J.E., and Idiart, M.A. (1995). Storage of 7 +/− 2 short-term memories in oscillatory subcycles. Science *267*, 1512–1515.

Magee, J.C., and Johnston, D. (1997). A synaptically controlled, associative signal for Hebbian plasticity in hippocampal neurons. Science *275*, 209–213.

Markram, H., Lubke, J., Frotscher, M., and Sakmann, B. (1997). Regulation of synaptic efficacy by coincidence of postsynaptic APs and EPSPs. Science *275*, 213–215.

McNaughton, B.L., Barnes, C.A., and O'Keefe, J. (1983). The contributions of position, direction, and velocity to single unit activity in the hippocampus of freely-moving rats. Exp. Brain Res. *52*, 41–49.

McNaughton, B.L., Barnes, C.A., Gerrard, J.L., Gothard, K., Jung, M.W., Knierim, J.J., Kudrimoti, H., Qin, Y., Skaggs, W.E., Suster, M., and Weaver, K.L. (1996). Deciphering the hippocampal polyglot: the hippocampus as a path integration system. J. Exp. Biol. *199*, 173–185.

Mehta, M.R., Barnes, C.A., and McNaughton, B.L. (1997). Experience-dependent, asymmetric expansion of hippocampal place fields. Proc. Natl. Acad. Sci. USA *94*, 8918–8921.

Mehta, M.R., Lee, A.K., and Wilson, M.A. (2002). Role of experience and oscillations in transforming a rate code into a temporal code. Nature *417*, 741–746.

Muller, R.U., Stead, M., and Pach, J. (1996). The hippocampus as a cognitive graph. J. Gen. Physiol. *107*, 663–694.

Nadasdy, Z., Hirase, H., Czurko, A., Csicsvari, J., and Buzsaki, G. (1999). Replay and time compression of recurring spike sequences in the hippocampus. J. Neurosci. *19*, 9497–9507.

Nakazawa, K., Quirk, M.C., Chitwood, R.A., Watanabe, M., Yeckel, M.F., Sun, L.D., Kato, A., Carr, C.A., Johnston, D., Wilson, M.A., and Tonegawa, S. (2002). Requirement for hippocampal CA3 NMDA receptors in associative memory recall. Science *297*, 211–218.

O'Keefe, J., and Nadel, L. (1978). The Hippocampus as a Cognitive Map (Oxford: Oxford University Press).

O'Keefe, J., and Recce, M.L. (1993). Phase relationship between hippocampal place units and the EEG theta rhythm. Hippocampus *3*, 317–330.

Redish, A.D., and Touretzky, D.S. (1997). Cognitive maps beyond the hippocampus. Hippocampus *7*, 15–35.

Samsonovich, A., and McNaughton, B.L. (1997). Path integration and cognitive mapping in a continuous attractor neural network model. J. Neurosci. *17*, 5900–5920.

Samsonovich, A.V., and Ascoli, G.A. (2005). A simple neural network model of the hippocampus suggesting its pathfinding role in episodic memory retrieval. Learn. Mem. *12*, 193–208.

Scoville, W.B., and Milner, B. (1957). Loss of recent memory after bilateral hippocampal lesions. J. Neurol. Neurosurg. Psychiatry *20*, 11–21.

Skaggs, W.E., McNaughton, B.L., Wilson, M.A., and Barnes, C.A. (1996). Theta phase precession in hippocampal neuronal populations and the compression of temporal sequences. Hippocampus *6*, 149–172.

Squire, L.R. (1992). Memory and the hippocampus: a synthesis from findings with rats, monkeys, and humans. Psychol. Rev. *99*, 195–231.

Treves, A., and Rolls, E.T. (1992). Computational constraints suggest the need for two distinct input systems to the hippocampal CA3 network. Hippocampus *2*, 189–199.

Tsodyks, M. (1999). Attractor neural network models of spatial maps in hippocampus. Hippocampus *9*, 481–489.

Tsodyks, M.V., Skaggs, W.E., Sejnowski, T.J., and McNaughton, B.L. (1996). Population dynamics and theta rhythm phase precession of hippocampal place cell firing: a spiking neuron model. Hippocampus *6*, 271–280.

Tulving, E. (1969). Retrograde amnesia in free recall. Science *164*, 88–90.

Tulving, E. (1972). Episodic and semantic memory. In Organization of Memory, D.W. Tulving, ed. (New York: Academic), pp. 382–403.

Wallenstein, G.V., and Hasselmo, M.E. (1997). GABAergic modulation of hippocampal population activity: sequence learning, place field development, and the phase precession effect. J. Neurophysiol. *78*, 393–408.

Wang, X.J. (2002). Pacemaker neurons for the theta rhythm and their synchronization in the septohippocampal reciprocal loop. J. Neurophysiol. *87*, 889–900.

Williams, T.L., Sigvardt, K.A., Kopell, N., Ermentrout, G.B., and Remler, M.P. (1990). Forcing of coupled nonlinear oscillators: studies of intersegmental coordination in the lamprey locomotor central pattern generator. J. Neurophysiol. *64*, 862–871.

Wills, T.J., Lever, C., Cacucci, F., Burgess, N., and O'Keefe, J. (2005). Attractor dynamics in the hippocampal representation of the local environment. Science *308*, 873–876.

Wilson, M.A., and McNaughton, B.L. (1993). Dynamics of the hippocampal ensemble code for space. Science *261*, 1055–1058.

Wilson, M.A., and McNaughton, B.L. (1994). Reactivation of hippocampal ensemble memories during sleep. Science *265*, 676–679.

Yamaguchi, Y., Aota, Y., McNaughton, B.L., and Lipa, P. (2002). Bimodality of theta phase precession in hippocampal place cells in freely running rats. J. Neurophysiol. *87*, 2629–2642.

Zugaro, M.B., Monconduit, L., and Buzsaki, G. (2005). Spike phase precession persists after transient intrahippocampal perturbation. Nat. Neurosci. *8*, 67–71.